

Laboratory experiment of the structural sensing method using the accurate artificial vibrator



Masayuki Saeki ^{a,*}, Tatsuya Kurihara ^a, Mika Tsukahara ^a, Takahiro Ohtani ^b

^a Department of Civil Engineering, Tokyo University of Science, 2641 Yamazaki, Noda-shi, Chiba, Japan

^b Graduate School of Information Science, Nagoya University, Furo-cho, Chikusa-ku, Nagoya 464-8601, Japan

ARTICLE INFO

Article history:

Received 20 May 2014

Received in revised form 9 January 2015

Accepted 26 March 2015

Available online 9 April 2015

Keywords:

Structural sensing method

Accurate artificial vibrator

Green function

ARX method

ABSTRACT

This paper presents a structural sensing method using the accurate artificial vibrator and shows the results of vibration experiments in laboratory scale. The accurate artificial vibrator generates harmonic forces by rotating an eccentric mass. Since the rotation is accurately controlled by means of a phase control type servomotor, the vibrator generates accurate harmonic forces periodically. The phase information obtained from the servomotor let us calculate the force function precisely. Applying Auto-Regressive eXogenous (ARX) model to the time series of force function and measured displacement responses yields the Green function of a target structure. In this research, we investigated the performance of prototype system and developed the Green function estimation method. We also conducted laboratory scale vibration tests in which the prototype system was applied to a two-meter simple beam. The estimated Green function was simulated by the analysis of Finite Element Method (FEM) and its structural model was successfully determined.

© 2015 Elsevier Ltd. All rights reserved.

1. Introduction

Deterioration of civil infrastructures is recognized as an important problem in advanced nations. It is considered unrealistic to reconstruct all of aged civil infrastructures for financial reason. Therefore, maintenance and management of civil infrastructures are needed to decrease their life cycle cost. In order to maintain civil infrastructures effectively, it is important to assess their current condition quantitatively. Therefore, various Structural Health Monitoring (SHM) systems have been studied by many researchers [2,4,5,24].

Vibration-based damage detection method might be a possible solution to estimate health condition of civil infrastructure, because natural frequencies, modal damping factors, mode shapes and also frequency response function reflect the mechanical condition such as the stiffness and boundary condition. One of the important issues of the vibration-based damage detection is variations of dynamic characteristics due to a temporal change of environmental condition [5]. Ambient vibration, which may be excited by a traffic or wind, is analyzed to estimate vibration characteristics in many studies. In general, ambient vibration is

assumed as white even though it depends on the source and then varies in case. Therefore, it is considered difficult to detect a small change of vibration characteristics accurately when the ambient vibration is analyzed. Therefore, an artificial vibrator, which is able to generate very accurate and stable forces, is needed.

Other important issue of vibration based damage detection is the limitation of the number of sensors [2]. However, in recent years, wireless sensor network is intensively studied in a research field of SHM to integrate an efficient monitoring system which allows us to deploy a number of sensors to a target structure. Wireless sensor network is a system consisting of a server (coordinator) and many sensor nodes (end devices) which have a radio communication module, physical sensors, a Micro-Processor Unit (MPU), and a small battery. This system enables us to decrease the installation and maintenance costs of SHM system and also to deploy many sensors to a target structure in high spatial resolution.

The authors have been developing a structural sensing system using the accurate artificial vibrator and wireless sensor network [11]. In this system, the accurate artificial vibrator generates harmonic forces and vibrates a target structure periodically. The wireless sensor nodes measure the acceleration responses as synchronizing with the vibrator. Because the excited forces are very accurate and stable, the Green functions of a target structure are accurately estimated. And also, measuring the responses at

* Corresponding author. Tel.: +81 4 7124 1501.

E-mail addresses: saeki@rs.noda.tus.ac.jp (M. Saeki), otani@hpc.itc.nagoya-u.ac.jp (T. Ohtani).

many points with the wireless sensor network provides a great quantity of information. The accurate Green functions obtained at many measuring points may improve accuracy and spatial resolution of damage detection.

The objective of this research is to demonstrate that the proposed method is able to estimate the Green function of a target structure very accurately. In this research, we first investigated the performance of prototype system and described a mathematical model of displacement response excited by the accurate artificial vibrator using Auto-Regressive eXogenous (ARX) model. We also carried out basic vibration tests in laboratory scale for demonstration of the present method. In the experiment, a prototype of the accurate artificial vibrator was applied to a two-meter simple beam supported by roller bearings. The displacement response was measured using wireless sensor nodes and a laser displacement meter. Analyzing the time series of displacements and force function with ARX method yields the Green functions from an excitation point to sensors. The Green function obtained from the laboratory scale experiment was successfully simulated by Finite Element Method (FEM) analysis.

2. Previous research

Structural health monitoring is performed to determine the location and severity of damage in a civil infrastructure. Various methods are proposed by many researchers. In general, these methods can be classified as local-damage detection method and global-damage detection method [24]. Local-damage detection methods are conducted to determine the exact location and extent of the damage like a crack in a part of damaged structure. On the other hand, global-damage detection methods detect damage throughout the whole structure by investigating spatial or temporal variation of vibration responses [4]. This paper focuses on the global-damage detection method. A review of papers related to the vibration-based global structural health monitoring can be found in Doebeling et al. [5], Chang et al. [4], Carden and Fanning [2], and Yan et al. [24].

Global-damage detection methods can be further classified as methods based on the dynamic characteristics of structure and methods based on online measured response signal of structure [24]. One of the former examples is model updating. This method adjusts the analytical mass and stiffness matrices of structure so that the analytical modal properties agree with the modal properties estimated from the measured responses. Cha and de Pillis presents a model updating method which updates the analytical model of structure by using additional information obtained from the operation of adding known masses to the physical structure [3]. Bernal develops other damage detection method using Damage Locating Vectors (DLVs). This method first estimates modal properties by analyzing the measured responses and assembles the flexibility matrices at sensor locations from the estimated modal properties. DLVs are calculated from the singular value decomposition of flexibility matrix [1]. Nagayama et al. develop a structural identification method consisting of vibration modes identification and inverse analysis of structural properties from the identified modes. They apply the developed method to the ambient vibration measurements of a full-scale suspension bridge, determine the mode characteristics, and detect changes in the structural properties [16]. The accuracy of system identification depends on the arrangement of sensors. So the sensor deployment can be treated as an optimization problem. Kripakaran and Smith present approaches for design of initial sensor deployment and the iterative placement of sensors for model filtering and damage identification. This method first predicts the analytical responses of structural models with possible damage scenarios and then investigates the histogram of model predictions. The sensor

deployment is determined so that the number of structural models effectively decreases [10]. Raich and Liszkai present a multi-objective optimization approach which minimizes the number of sensors while maximizing the sensitivity of the frequency response functions (FRFs) collected at each specified sensor location with respect to all possible damaged structural elements [19].

It is often criticized that the accurate structural model cannot be obtained for existing structures and also that the modal analysis is time consuming and expensive. Therefore, online measured response based method, that is, structural model-free method is studied. Posenato et al. present two statistical approaches of moving principal component analysis and moving correlation analysis to identify and localize anomalous behavior in civil infrastructure [18]. Sohn and Farrar present a damage diagnosis method in which measured acceleration time series are solely analyzed to find out the difference from the time series predicted using the closet AR-ARX model. The AR-ARX models are determined in advance from the acceleration responses of non-damaged structure measured under various environmental conditions. The increase in residual errors would be maximized at the sensors instrumented near the actual damage locations [21]. Fasel et al. investigate the applicability of a frequency domain ARX model to measured responses to detect non-linearity of damaged structure. It is shown that the vibration-based method is, while able to detect anomaly when damage is present in structure, is unable to localize the damage. They also investigate the applicability of a frequency domain ARX model to the data obtained from an impedance-based active sensing method [17] and show that their method is able to localize the damage [6].

The accuracy and spatial resolution of damage detection highly depends on the sensor deployment. WSN is expected to improve the accuracy and spatial resolution of damage detection because WSN decreases installation and maintenance cost of sensor networks and thus a large number of sensors can be deployed in a target structure [14]. One of the critical issues of WSN is how to decrease energy consumption of wireless sensor nodes. Lynch et al. present a power-efficient wireless structural monitoring system with local data processing. The developed wireless sensor node is able to measure time-history response using a Micro Electronic Mechanical Systems (MEMS) accelerometer and perform computational tasks associated with system identification and damage detection instead of transmitting the raw measured response to a central server. The computation on the sensor node results in the saving of electricity [13]. Smarsly and Law present an agent migrations approach for performing simple resource-efficient routines to continuously analyze, aggregate, and transmit the sensor data to a central server [20]. Reliable data transportation, compression of data size, and time-synchronization are also important features of WSN. Xu et al. develop a WSN system, called Wisden, for structural monitoring which implements the scheme achieving the above three features. In their system, a data time-stamping method is implemented to avoid global clock synchronization [22]. Kim et al. deploy 64 wireless sensor nodes on the Golden Gate Bridge, measure ambient vibration using MEMS accelerometers, and estimate FRFs and mode shapes. It is shown that the collected data agrees with theoretical models and previous studies of the bridge [9]. Kijewski-Correa et al. present a WSN system with multi-scale approach. In their system, once globally distributed wireless sensor nodes detect anomalies by analyzing the acceleration responses, the system measures strain responses using sub-networks in the vicinity of suspected damage location. The time series of acceleration and strain responses are described using an ARMA model. The damage is detected based on the residual error of the ARMA analysis [8].

The approaches mentioned above are mostly based on the analysis of ambient vibration. Since an artificial excitation is

considered difficult and unrealistic for a large scale structure, ambient vibration is often used for the system identification and damage detection although the accurate excitation is able to improve the signal-to-noise ratio. Lim et al. present a structural damage detection method using real-time modal parameter identification algorithm. In their experiment, a small truss structure is vibrated using the piezoceramic active strut which substituted for a diagonal truss member. The force transducer signal and measured acceleration signal are analyzed together to estimate FRFs at sensor locations by using the developed algorithm [12]. Yamaoka et al. develop the seismic source of an accurately controlled routine-operated signal system, called ACROSS, to monitor a spatial and temporal change of seismic fault in the crust. The magnitude of force is about 200 kN at 25 Hz. The accurate artificial vibrator presented in this paper is recognized as a small type of the ACROSS source [23].

3. Overview of the proposed structural sensing method using the accurate artificial vibrator and wireless sensor network

3.1. Overview of the proposed structural sensing method

A schematic view of the structural sensing method proposed in this paper is shown in Fig. 1.

The accurate artificial vibrator produces the frequency modulated force periodically by rotating an eccentric mass. Since the rotation is accurately controlled, the generated forces are very stable. The force function $f(t)$ is calculated by substituting the rotational phase $\phi(t)$ into the expression of centrifugal force:

$$f(t) = mr\omega(t)^2 e^{i \int \omega(t) dt} = mr \left(\frac{d\phi}{dt} \right)^2 e^{i\phi(t)} \quad (1)$$

where mr is the first moment of eccentric mass and $\omega(t)$ is the angular frequency. The rotational frequency of eccentric mass is periodically modulated with a specified time interval T_s that is frequency modulation period. This frequency modulation enables us to obtain several frequency components of harmonic forces simultaneously.

The accurate artificial vibrator also broadcasts a trigger signal at every start of the frequency modulation. This means what the trigger signal is broadcasted every T_s seconds. The wireless sensor node starts sampling data just after receiving the trigger signal and collects data during an interval of frequency modulation T_s . After the interval, it waits the next trigger signal. This operation permits the wireless sensor nodes to be synchronized with the accurate artificial vibrator. The observed time series data are

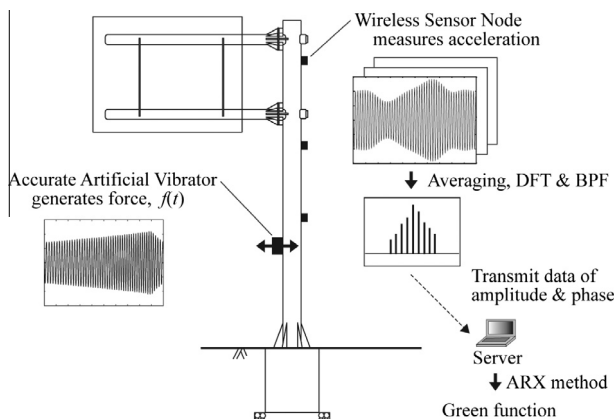


Fig. 1. Schematic view of the proposed structural sensing method using the accurate artificial vibrator and wireless sensor network.

averaged in time on the sensor node to improve the signal to noise ratio.

After finishing observation, the sensor node calculates the amplitude and phase of frequency components corresponding to the excited forces by applying Discrete Fourier Transform (DFT) to the averaged time series data. Since the vibrator generates a limited number of frequency components, the data amount can be drastically compressed. The compressed data, which corresponds to a band-pass filtered FRF, is transmitted to the server through wireless communication.

In the server, the FRF is divided by $-\omega^2$ to convert the acceleration data to displacement, and Inverse Discrete Fourier Transform (IDFT) is applied to the converted data to obtain a band-pass filtered displacement time series data $u_b(t)$. The same band-pass filter is also applied to the force function $f(t)$ and then a band-pass filtered force function $f_b(t)$ is obtained. Analyzing $u_b(t)$ and $f_b(t)$ together with ARX method yields an estimation of Green function.

3.2. Prototype of accurate artificial vibrator

Fig. 2 shows a prototype of the accurate artificial vibrator developed in this research. The vibrator consists of an eccentric mass, a phase control type servomotor and the control pulse generator which also has micro-controller and wireless communication module. The first moment of the eccentric mass shown in Fig. 2 is 9.69×10^{-5} kg m which excites a force of 1.17 N at a constant frequency of 20 Hz. The eccentric mass is changeable, and hence the magnitude of force is variable. Total weight of the excitation part (servomotor, eccentric mass, a frame) is about 2.5 kg.

The micro-controller mounted on the pulse generator outputs control pulses to the servomotor. The servomotor rotates an eccentric mass according to the count of pulses. Frequency modulation is attained by varying the pulse speed. Fig. 3 shows an example of temporal variation of modulated frequency. In this example, the frequency modulation period T_s is set to be 10 s. The rotational frequency is linearly increased from about 4.5 Hz to 5.5 Hz for 9 s and decreased back to 4.5 Hz for 1 s. The servomotor employed in the prototype is operational up to 50 Hz.

Fig. 4 shows the force function $f(t)$ and its Fourier spectrum in case of the frequency modulation shown in Fig. 3. As shown in Fig. 4a, the magnitude of force is gradually increased for 9 s and decreased to the initial value for 1 s. The Fourier spectrum has signals every 0.1 Hz because the period of force function is 10 s in this example. The frequency components from 4.5 Hz to 5.5 Hz are mostly excited in this example.

If the torque of servomotor is insufficient or the feedback control does not work effectively, the rotational phase error becomes large. As a result, the force function cannot be determined precisely. So, it is important to verify the temporal stability of the

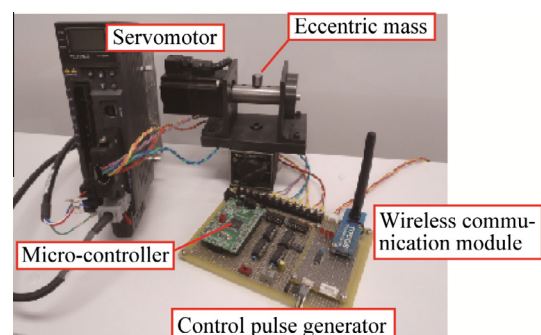


Fig. 2. Prototype of the accurate artificial vibrator.

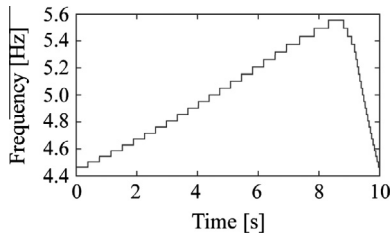


Fig. 3. An example of temporal variation of modulated frequency.

force function. Actual rotational phase can be obtained by counting the A-phase pulses which is provided from the encoder of servomotor. In the prototype, the encoder A-phase is set to output 10,240 pulses a rotation, that is, a single A-phase encoder pulse corresponds to $2\pi/10,240$ radian. So, the rotational phase $\phi(t)$ is calculated by multiplying the counts by $2\pi/10,240$ radian. The excited force function is estimated by substituting the phase $\phi(t)$ into Eq. (1). In the measurement, the counts of encoder A-phase pulses are recorded every 1 ms. The residual error of the force function, which is defined as $\|f(t) - f_e(t)\|$ where $f_e(t)$ is the averaged force function, is investigated. Fig. 5 shows a temporal variation of the residual error rate. The force function is very stable and the residual error rate is less than 1% during 1 h operation.

3.3. Prototype of wireless sensor node

Fig. 6 shows a prototype of wireless sensor node developed in this research. The sensor node consists of a wireless communication module, a tri-axial MEMS accelerometer, three 16 bit Analog to Digital Converters (ADC) and a small battery. The wireless communication module employed in the prototype has a 32 bit micro-computer and 128 kbyte Random Access Memory (RAM), and its maximum communication speed is 250 kbps. The embedded software of the module is developed based on IEEE802.15.4 protocol in this study. The prototype of sensor node goes into wait mode after initialization. It starts sampling data when it receives the trigger signal and measures acceleration response at sampling rate of 100 Hz. After collecting 1000 samples which corresponds to 9.99 s, it stops the acquisition and returns back to wait mode again. The collected responses are immediately averaged on the sensor node. After averaging the measurements sufficient times, the amplitudes and phases of frequency components corresponding to the force function are calculated and transmitted to the server.

In order to obtain the time series of acceleration response accurately, the acquisition of acceleration response should be synchronized with the eccentric mass rotation. However, in this system, the time synchronization is attained by broadcasting the trigger signals from the accurate artificial vibrator. And the wireless sensor node starts sampling data when it receives the trigger signal.

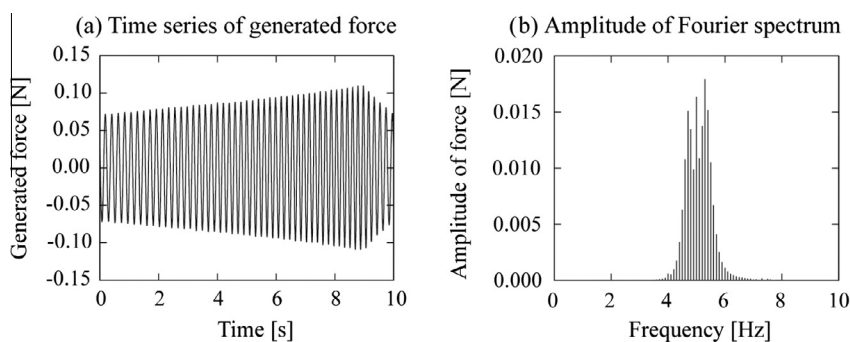


Fig. 4. Force function $f(t)$ and its Fourier spectrum in case of the frequency modulation shown in Fig. 3.

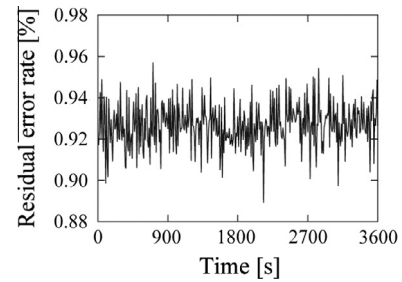


Fig. 5. Temporal variation of the residual error rate of the forces function.

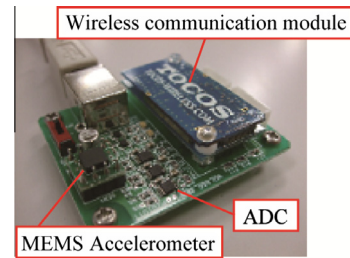


Fig. 6. Prototype of wireless sensor node equipped with MEMS accelerometer and 16 bit ADCs.

In this process, the wireless sensor node needs a millisecond order processing time to receive a wireless communication packet and check the packet contents whether the packet is trigger signal or not. So, we measured the processing time and investigated the accuracy of delay time.

Fig. 7 shows a fluctuation of the acquisition delay time which is measured using the current version program of wireless sensor node. The maximum and the minimum delay time are 1.397 and 1.376 ms, respectively. The fluctuation seems random and the range of fluctuation is 21 ms. Since the observed acceleration measurements are averaged, the fluctuation might be suppressed to a few microseconds. And also, measuring the delay time of other wireless sensor nodes gives almost the same result. Therefore, phase estimation error due to the delay time of data sampling can be corrected after the acceleration measurement.

4. Green function estimation using ARX method

4.1. Mathematical model of displacement response excited by the accurate artificial vibrator

A dynamic displacement field of linear elastic body can be discretized by means of finite element method.

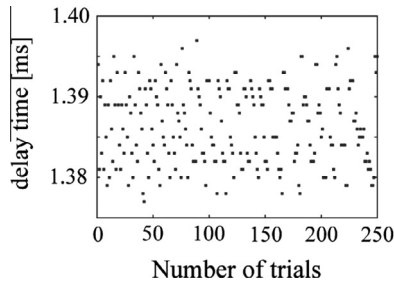


Fig. 7. Fluctuation of the acquisition delay time measured using the developed wireless sensor node.

$$[\mathbf{M}]\ddot{\mathbf{U}}(t) + [\mathbf{C}]\dot{\mathbf{U}}(t) + [\mathbf{K}]\mathbf{U}(t) = \mathbf{F}(t) \quad (2)$$

where $[\mathbf{M}]$ is mass matrix, $[\mathbf{C}]$ is damping matrix, $[\mathbf{K}]$ is stiffness matrix, $\mathbf{U}(t)$ is displacement vector with N degree of freedom and $\mathbf{F}(t)$ is force vector. Since the accurate artificial vibrator is considered as a point force, the force vector can be expressed as

$$\mathbf{F}(t) = \{0, \dots, 0, f_s(t), 0, \dots, 0\}^T \quad (3)$$

where $f_s(t)$ is the force function applied at s th degree of freedom.

The response of multi-degree-of-freedom systems can be decoupled into modal equations by modal analysis [15]. According to the proper orthogonal mode decomposition [7], the displacement vector can be expressed as a summation of modes:

$$\mathbf{U}(t) = \sum_{j=1}^N \mathbf{v}_j q_j(t) = [\mathbf{V}]\mathbf{Q}(t) \quad (4)$$

where \mathbf{v}_j and $q_j(t)$ represent j th mode shape and its time dependence, respectively. The coefficient matrices $[\mathbf{M}]$, $[\mathbf{K}]$ and also $[\mathbf{C}]$ can be diagonalized with the matrix $[\mathbf{V}]$ if $[\mathbf{C}]$ is modeled as $[\mathbf{C}] = \alpha[\mathbf{M}] + \beta[\mathbf{K}]$. Substituting Eq. (4) into Eq. (2) and multiplying the matrix $[\mathbf{V}]^T$ from the left yields the following modal equations:

$$m_j \ddot{q}_j(t) + c_j \dot{q}_j(t) + k_j q_j(t) = v_{sj} f_s(t), \quad j = 1, \dots, N \quad (5)$$

where m_j , c_j and k_j are the j th components of the diagonalized mass matrix, damping matrix and stiffness matrix, respectively. Applying Fourier transform to Eq. (5) yields the solution in frequency domain. Therefore, the Green function from the excitation point s to a sensor i is expressed as

$$G_{is}(\omega) = \frac{U_i(\omega)}{F_s(\omega)} = \sum_{j=1}^N \frac{v_{ij} Q_j(\omega)}{F_s(\omega)} = \sum_{j=1}^N \frac{v_{ij} v_{sj}}{-m_j \omega^2 + i c_j \omega + k_j} \quad (6)$$

where ω is angular frequency, $U_i(\omega)$, $Q_j(\omega)$ and $F_s(\omega)$ are the Fourier spectrum of $u_i(t)$, $q_j(t)$ and $f_s(t)$, respectively. In general, the Green function of civil structures can be approximated as a summation of less number of modal solutions because the amplitude of each mode rapidly decreasing with angular frequency. Therefore, the Green function might be expressed as a function having $2M$ poles and $2M - 2$ zeros, where M is a small natural number.

4.2. Estimation of Green function using ARX model

A displacement response of linear elastic body $u(t)$ excited by a force function $f(t)$ is modeled by using the following ARX model:

$$\sum_{n=0}^{2M} a_n u(t - n\Delta t) = \sum_{n=0}^{2M-2} b_n f(t - n\Delta t) + \varepsilon(t) \quad (7)$$

where a_n and b_n are ARX coefficients, Δt is a sampling interval, and $\varepsilon(t)$ is white noise. Applying Z-transform to Eq. (7) and estimating frequency transfer function yields the same expression to Eq. (6) which has $2M$ poles and $2M - 2$ zeros. So, the model of Eq. (7) is

applicable if a structure satisfies the following conditions; (i) target structure is linear elastic body, (ii) damping matrix is proportional to mass and stiffness matrices, and (iii) noise is white.

In the proposed structural sensing method, the first and second assumption could be considered acceptable because the magnitude of force is very small and then non-linear response might be negligible. On the other hand, the third assumption is not valid because the displacement response and force function are band-pass filtered and the noise is not already white yet. However, as mentioned in the following section, the Green function seems to be estimated successfully by using Eq. (7).

5. Simple beam vibration test in laboratory scale

5.1. Overview of simple beam vibration test

We conducted two different experiments in this research. The objective of the first experiment was to confirm whether the Green function estimated by the present method could be accurately simulated by FEM analysis or not. Therefore, in the first experiment, a laser displacement meter was employed as a sensor. Besides, the effects of temperature and deployment condition of accurate artificial vibrator were also investigated. In the second experiment, the responses were measured using 8 wireless sensor nodes with a laser displacement meter to evaluate the accuracy of Green functions estimated from the measured data of wireless sensor nodes.

Fig. 8 shows an arrangement of simple beam vibration test. In the experiment, a rolled steel SS400 plate was supported by roller bearings. The length of steel plate was about 2100 mm, the width was 100 mm and the height was 10 mm. The span of simple beam was set to be 2000 mm. The accurate artificial vibrator was fixed at the center of the simple beam by means of a powerful magnet. In this condition, the eigen frequency of the first bending vibration mode was about 5 Hz. Therefore, in the experiment, the accurate artificial vibrator was operated with the frequency modulation from 4.5 to 5.5 Hz as shown in Fig. 3. A laser displacement meter was settled at 750 mm from a support. In case of measuring the second mode, the vibrator and laser displacement meter were differently arranged. In this paper, only the result of the first mode is shown.

In the first experiment, the displacement response was measured using a laser displacement meter at a sampling rate of 1 kHz as time-synchronizing with the accurate artificial vibrator. After several hours of operation for waiting for boundary condition to be stable, we manually turned off and on the switch of vibrator's powerful magnet every 5 min to investigate the effect of friction between the vibrator and the simple beam because the friction was considered to enlarge the bending stiffness locally and thus increase eigen frequency. After that, we also collected displacement response continuously for more several hours to study the effect of temperature on the eigen frequency. The temperature of

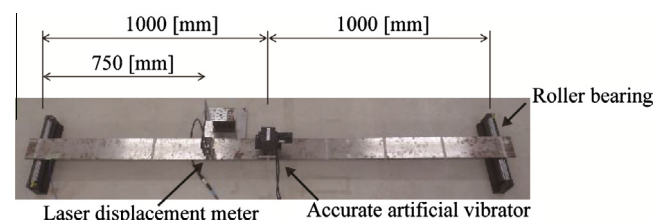


Fig. 8. Arrangement of simple beam vibration test in case of the first bending vibration mode.

simple beam was measured around a roller bearing by means of a thermocouple.

In the second experiment, a wireless sensor node was located at the point next to the measuring point of laser displacement meter. The operational condition of laser displacement meter and accurate artificial vibrator was the same to that of the first experiment. In a single measurement, a wireless sensor node measured acceleration response for 10 s at a sampling rate of 100 Hz 100 times. After averaging the measured responses, the node calculated the frequency components of Fourier spectrum and transmitted the data to a central server as mentioned in Section 3.3. This observation was carried out 10 times for each sensor node and 8 sensor nodes were tested. Therefore, 80 data sets were obtained. The collected data sets were converted to the time series data of displacement in a post-processing.

5.2. Green function estimated by means of ARX method

In the analysis, the force function is calculated from A-phase pulse counts and applied a band-pass filter. The displacement time series measured by the laser displacement meter is segmented by 10 s and the segments are transformed by applying the same band-pass filter. The band-pass filtered segments and force function are analyzed together with ARX method to estimate Green functions. Fig. 9 shows an example of estimated Green function. In the figure, the solid line represents the Green function estimated by ARX method, and the x-marks are the results calculated by the expression of $U(\omega)/F(\omega)$ where $U(\omega)$ and $F(\omega)$ are the Fourier spectrum of measured displacement and force function, respectively. The Green function estimated by ARX method is very consistent with the estimation of $U(\omega)/F(\omega)$.

5.3. Effect of friction between the vibrator and the steel plate on eigen frequency

Fig. 10 shows a temporal variation of the estimated eigen frequency when the switch of powerful magnet fixing the vibrator on the steel plate was turned off and on. When the switch is turned off, the eigen frequency is decreased by about 0.04% in this experiment. That means what the friction between the powerful magnet and the steel plate provides a bending resistance. However, the amount of frequency change is not stable and the mechanism is not made clear yet.

The eigen frequency shown in Fig. 10 gradually varies with time except for the moment of turning the switch of powerful magnet. This is due to the temporal change of temperature of simple beam. A small impact due to manual operation also influences the eigen frequency. Even though the switch of powerful magnet was carefully turned on and off, the manual operation might change the boundary condition of simple beam.

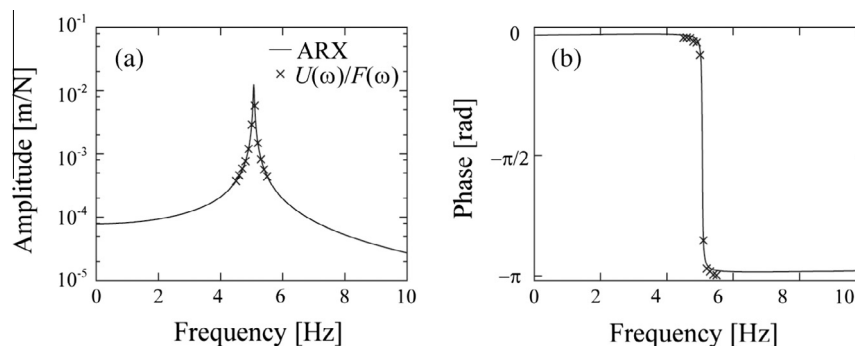


Fig. 9. An example of estimated Green function (amplitude and phase).

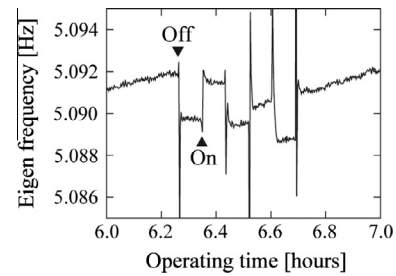


Fig. 10. Temporal variation of the estimated eigen frequency in case of switching on and off the vibrator's powerful magnet.

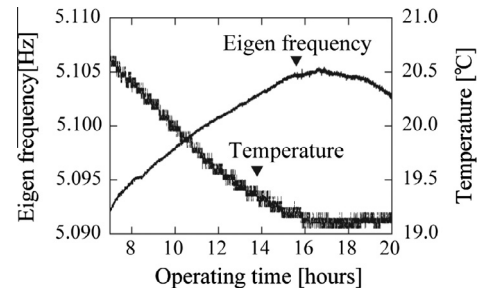


Fig. 11. Temporal variation of the estimated eigen frequency and the measured temperature.

5.4. Effect of temperature on eigen frequency

Fig. 11 shows a temporal variation of the estimated eigen frequency and the measured temperature of simple beam. This is the continuation from the data shown in Fig. 10. The estimated eigen frequency gradually increases with the decrease of temperature. The change of temperature might vary the Young's modulus, size, and mass density of the steel plate. However, considering the thermal expansion coefficient of steel, it is difficult to explain the temporal variation of eigen frequency by the change of size and mass density. Therefore, it is considered that the bending stiffness becomes high when Young's modulus increases with the decrease of temperature.

5.5. Accuracy of Green functions estimated from the data of wireless sensor nodes

To evaluate the estimation accuracy of Green functions obtained from the data of wireless sensor node, the results are compared to that of laser displacement meter. The sensitivity of MEMS accelerometer mounted on the wireless sensor nodes is calibrated by comparing with the results of laser displacement meter. Table 1 shows the residual error rate of eigen frequency,

Table 1
Standard deviation of eigen frequency, damping ratio, and peak amplitude of Green functions [Units: %].

Sensor ID	1	2	3	4	5	6	7	8
Eigen frequency	0.006	0.007	0.008	0.010	0.003	0.003	0.004	0.005
Damping ratio	2.07	2.22	3.76	9.27	1.86	3.43	2.84	2.27
Peak amplitude	2.05	2.13	2.76	8.26	2.10	1.37	2.00	2.09

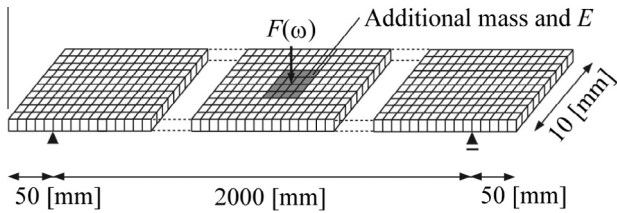


Fig. 12. Schematic view of the finite element model used in the analysis.

damping ratio, and peak amplitude of the estimated Green functions. In this evaluation, the results of laser displacement meter are assumed to be true value. Excluding the results of sensor ID 4, the residual error rate of eigen frequencies, damping ratios, and peak amplitudes are less than 0.01%, 3.5%, and 3.0%, respectively. Since some of the converted displacement time series of ID 4 are very different from the others, it is considered that the sensor ID 4 might have some trouble in the experiment.

6. Estimation of structural model using FEM analysis

6.1. Finite element model

To validate the Green function estimated by the developed prototype system, we conduct finite element analysis and compare it with the experimental results. The finite element model used in this analysis is shown in Fig. 12. The steel plate is divided into 2100 (=210 × 10 × 1) elements. The second order solid element is used for simulating a bending deformation. Since a single element has 20 nodes, the total number of nodes is 15,053. As a boundary condition, the displacement of the node corresponding to the bearing position is fixed in three directions at one side, and the displacement at another side is fixed in the transversal and vertical direction and free in the axial direction. The damping matrix proportional to the stiffness matrix is introduced in the analysis. The material parameters are assumed to be uniform except for the elements corresponding to the position of vibrator. The density ρ is set to be $7.85 \times 10^3 \text{ kg/m}^3$, and the Poisson’s ratio is 0.3. The Young’s modulus E is treated as an unknown parameter in this analysis for fitting the eigen frequency of numerical simulation to that of experimental result. The density and

Young’s modulus of the element corresponding to the vibrator position are increased to represent the mass of vibrator and the effect of friction between the vibrator and the steel plate, respectively. The damping ratio is set to be 0.004 which is obtained from the analysis with ARX method.

6.2. Structural model determination

Green function is simulated by using the finite element model mentioned in Section 6.1. In the analysis, Young’s modulus is manually determined so that the eigen frequency of Green function agrees with the result of measurement.

A Green function is first calculated with a typical value of Young’s modulus $E = 206 \text{ GPa}$ for background and relatively higher value for the elements corresponding to the vibrator location. The additional value of Young’s modulus is determined by trial and error. The change in eigen frequency due to the powerful magnet of vibrator, that is about 0.04% in the experiment, can be represented by increasing the Young’s modulus of sensor location by 5 GPa. Next, the Young’s modulus of background is changed by trial and error until the eigen frequency is identical with the experimental result. As a result, Young’s modulus is determined as $E = 209 \text{ GPa}$ for background and $E = 214 \text{ GPa}$ for elements corresponding to the vibrator position.

Fig. 13 shows the Green functions obtained from the numerical simulation (x-marks) and the experiment (solid line). The figure on the left-hand side represents the amplitude and that on the right-hand side is the phase, respectively. The figure shows that the numerical result seems to be in good agreement with the experimental result. The residual error rate is 4.56%. We also tested the second mode, and the result shows good agreement. The other higher modes will be examined in a future study.

7. Conclusions

This paper presents the structural sensing method using the accurate artificial vibrator and the wireless sensor network. The accurate artificial vibrator generates very accurate harmonic forces and the wireless sensor network measures the acceleration response as time-synchronizing with the vibrator. Therefore, the force function and the displacement time series, which is converted from the data of wireless sensor node, are described as an

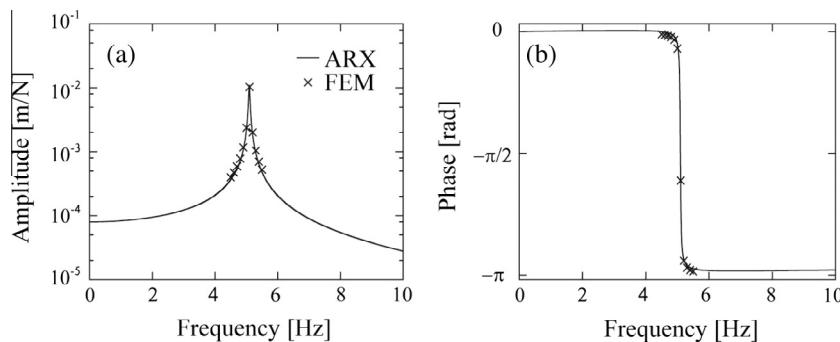


Fig. 13. Comparison between Green functions obtained from experiment and FEM analysis.

ARX model. By solving the ARX equations, Green functions are accurately estimated. The experimental results show that the residual error rate of eigen frequency, damping ratio, and peak amplitude of Green function obtained by the proposed method are less than 0.01%, 3.5%, and 3.0%, respectively. The numerical simulation also supports that the Green function is accurately obtained by the proposed method.

Because of the accuracy, the Green functions or the raw time series data obtained by means of the present method can be used as input data of the existing global-damage detection methods described in Section 2. In a future work, the existing global-damage detection method will be applied to the measurement of the present approach.

Application to real civil infrastructures is also important future work. Since the power of prototype vibrator is very small and the wireless communication range is short, it is difficult to apply the prototype system to a large civil infrastructure such as a suspension bridge. Therefore, we currently try to apply the preset method to the health monitoring of road signs as described in Fig. 1. Development of powerful vibrator for a large civil infrastructure is also a needed future work.

Acknowledgments

This study is supported by Grant-in-Aid for Scientific Research (C) of Japan Society for the Promotion of Science (JSPS) and is partly supported by Grant-in-Aid for Scientific Research (A) of JSPS.

References

- [1] D. Bernal, Load vectors for damage localization, *J. Eng. Mech.* 128 (1) (2002) 7–14.
- [2] E.P. Carden, P. Fanning, Vibration based condition monitoring: a review, *J. Struct. Health Monit.* 3 (4) (2004) 355–377.
- [3] P.D. Cha, L.G. de Pillis, Model updating by adding known masses, *Int. J. Numer. Eng.* 50 (2001) 2547–2571.
- [4] P.C. Chang, A. Flatau, S.C. Liu, Review paper: health monitoring of civil infrastructure, *Struct. Health Monit.* 2 (3) (2003) 257–267.
- [5] S.W. Doebling, C.R. Farrar, M.B. Prime, A summary review of vibration-based damage identification methods, *Shock Vib. Dig.* 30 (2) (1998) 91–105.
- [6] T.R. Fasel, H. Sohn, G. Park, C.R. Farrar, Active sensing using impedance-based ARX models and extreme value statistics for damage detection, *Earthq. Eng. Struct. Dyn.* 34 (2005) 763–785.
- [7] G. Kerschen, J.C. Golinval, Physical interpretation of the proper orthogonal modes using the singular value decomposition, *J. Sound Vib.* 249 (5) (2002) 849–865.
- [8] T. Kijewski-Correa, M. Haenggi, P. Antsaklis, Wireless sensor networks for structural health monitoring: a multi-scale approach, in: *Proc. of ASCE Structures Congress, 2006*, pp. 1–16.
- [9] S. Kim, S. Pakzad, D. Culler, J. Demmel, G. Fenves, S. Glaser, M. Turon, Health monitoring of civil infrastructures using wireless sensor networks, in: *Proc. of ISPN'07, Massachusetts, USA, 2007*.
- [10] P. Kripakaran, I.F.C. Smith, Configuring and enhancing measurement systems for damage identification, *Adv. Eng. Inform.* 23 (2009) 424–432.
- [11] T. Kurihara, M. Tsukahara, T. Saitou, K. Watanabe, M. Saeki, Structural sensing method using the accurate artificial vibrator and wireless sensor network, in: *Proceedings of ICCBEI, Tokyo, Japan, 2013*, pp. 21–27.
- [12] T.W. Lim, A. Bosse, S. Fisher, Structural damage detection using real-time modal parameter identification algorithm, *AIAA J.* 34 (11) (1996) 2370–2375.
- [13] J.P. Lynch, A. Sundararajan, K.H. Law, A.S. Kiremidjian, E. Carryer, Power-efficient wireless structural monitoring with local data processing, in: *Proceedings of the International Conference on Structural Health Monitoring, Tokyo, Japan, 2003*.
- [14] J.P. Lynch, Overview of wireless sensors for real-time health monitoring of civil structures, in: *Proc. of the 4th International Workshop on Structural Control and Monitoring, NY, USA, June 10–11, 2004*.
- [15] L. Meirovitch, *Principles and Techniques of Vibrations*, International ed., Prentice Hall, New Jersey, 1997.
- [16] T. Nagayama, M. Abe, Y. Fujino, K. Ikeda, Structural identification of a nonproportionally damped system and its application to a full-scale suspension bridge, *J. Struct. Eng.* 131 (10) (2005).
- [17] G. Park, H.H. Cudney, D.J. Inman, Impedance-based health monitoring of civil structural components, *J. Infrastruct. Syst.* 6 (2000) 153–160.
- [18] D. Posenato, F. Lanata, D. Inaudi, I.F.C. Smith, Model-free data interpretation for continuous monitoring of complex structures, *Adv. Eng. Inform.* 22 (2008) 135–144.
- [19] A.M. Raich, T.R. Liskai, Multi-objective optimization of sensor and excitation layouts for frequency response function-based structural damage identification, *Comput.-Aided Civ. Infrastruct. Eng.* 27 (2012) 95–117.
- [20] K. Smarsly, K.H. Law, A migration-based approach towards resource-efficient wireless structural health monitoring, *Adv. Eng. Inform.* 27 (2013) 625–635.
- [21] H. Sohn, C.R. Farrar, Damage diagnosis using time series analysis of vibration signals, *Smart Mater. Struct.* 10 (2001) 446–451.
- [22] N. Xu, S. Rangwala, K.K. Chintalapudi, D. Ganesan, A. Broad, R. Govindan, D. Estrin, A wireless sensor network for structural monitoring, in: *SenSys' 04, Baltimore, USA, 2004*.
- [23] K. Yamaoka, T. Kunitomo, K. Miyakawa, K. Kobayashi, M. Kumazawa, A trial for monitoring temporal variation of seismic velocity using an ACROSS system, *Island Arc* 10 (2001) 336–347.
- [24] Y.J. Yan, L. Cheng, Z.Y. Wu, L.H. Yam, Development in vibration-based structural damage detection technique, *Mech. Syst. Signal Process.* 21 (2007) 2198–2211.